Electronic Decoupling in Ground and Excited States of Asymmetric Biaryls

Martin Baumgarten,*,†,‡ Lileta Gherghel,† Jan Friedrich,† Martin Jurczok,§ and Wolfgang Rettig*,§

Max-Planck-Institute for Polymer Research, Ackermannweg 10, 55128 Mainz, Germany, and Institute for Physical and Theoretical Chemistry, Humboldt University Berlin, Bunsenstrasse 1, 10117 Berlin, Germany

Received: September 13, 1999; In Final Form: November 22, 1999

New asymmetric biaryls have been synthesized in order to clarify the conditions necessary for charge-transfer transitions in photoexcited neutral compounds and biradical formation in doubly charged ground-state species. A parallel behavior for both types of approaches is observed and explained with a simple coupling model allowing prediction of the intermoiety coupling strength. It is shown that for weakly coupled biaryls the monoions are connected with charge localization and the dications and dianions form thermally excited biradicals while the fluorescence data indicate biradicaloid excited states connected with partial charge separation. More strongly coupled biaryls, on the other hand, result in diamagnetic species for the doubly charged ground-state ions, and a charge-transfer contribution in the fluorescence spectra of the neutral compound is absent.

1. Introduction

There has been much interest in the design of organic materials that are suitable for electron transfer, electron storage, and the formation of high-spin states.[1−4] In this context, biaryls, oligoarylenes, and polyarylenes serve as important chromophores and electrophores.[5−8] In the case of biaryl compounds the main question deals with the magnitude of the interaction between the connected aromatic π-systems. The electronic coupling in bi- and oligoarylenes depends sensitively on the topology and geometry of the connected molecules, including the angle of torsion between them. If the coupling between the connected π-systems is strong, there will be resonance, and one can expect an extended π-system that can be described by a single minimum of the potential hypersurface as a result of strong overlap of the two minima for nearly planar conformations. When the molecule is singly charged, a complete charge delocalization in such biaryls and extended delocalization over several subunits in the higher oligomers are found as expected, and a second charging process leads to diamagnetic diions.

Medium and weakly coupled biaryls, on the other hand, can be described by double minima of the potential hypersurface with a conformation closer to perpendicular and with differently sized activation barriers between them. Here, the process of singly charging may lead either to delocalization of the charge/spin, induced by a fast self-exchange processes or to a charge and spin localization on one subunit. Further charging can lead to the generation of biradicals for the doubly charged ions. Earlier investigations of symmetric biaryls such as 9,9′-bianthryl (**1**)[5] or 1,1′-bipyrenyl (**2**)[8] have established that an electron exchange between the two subunits takes place in the singly charged species.[1,9] Similar to barrierless electron-transfer processes that can be described in terms of Marcus theory,[10−14] it is found that the electron transfer between the subunits of the above-mentioned symmetric biaryls often is temperature-independent. In the case of $\mathbf{1}^-$, generated by potassium reduction, a spin delocalization is observed for small anion concentrations.[5a] A further increase of the concentration of monocharged species $\mathbf{1}^-$ leads to a transition from a delocalized spin distribution over both subunits to a localization of the spin density on one subunit. In this mixture alternating line width phenomena in the EPR spectra sometimes have been erroneously interpreted as a kinetic process,[15a] although no temperature dependence can be found and this effect is independent of counterions as demonstrated also by electrochemical generation.[15b,c] In accord with these findings are descriptions by Gerson et al.[16a,b] for other symmetric bridged binaphthyls where a transition from a spin delocalized to a localized form upon increasing reduction was observed.[16a,b] This signifies that the increasing concentration of monoradicals hinders the spin exchange process. For $\mathbf{2}^-$, the electron hopping is independent of the concentration of charge-carrying molecules.[9,15b] In the case of the dianions, $\mathbf{2}^{2-}$ is diamagnetic and only $\mathbf{1}^{2-}$ exists as a biradicaloid species with paramagnetic properties. With the assumption that the magnitude of the bridgehead MO coefficients and the torsional angle controls the interaction between the two π-subunits, a consequent step is to investigate new asymmetric biaryl compounds with similar redox potentials to better understand the nature of the interactions between the coupled π-systems. A large progress would be possible if a general rule for the structural requirements could be found, which determines whether a strong or weak electronic coupling between the subunits is to be expected. In the case of the asymmetric biaryls, one has to deal with directly connected π-systems possessing different MO coefficients at the bridgehead carbon centers. Furthermore, the asymmetric biaryls differ from their symmetric analogues by unequal redox potentials and optical absorptions of the submoieties. In this respect, the central point deals with the question of whether an electron-hopping process can still be observed in the monoradical species. Moreover, it is of interest to compare the doubly charged symmetric and asymmetric biaryls with respect to the formation of biradicaloid states and with respect to a possible photoinduced

* To whom correspondence should be addressed.
† E-mail: baumgart@mpip-mainz.mpg.de.
‡ Max-Planck-Institute for Polymer Research.
§ Humboldt University Berlin.

10.1021/jp9932315 CCC: $19.00
Published on Web 01/22/2000

SCHEME 1: Molecular Structure of Symmetric and Asymmetric Biaryls

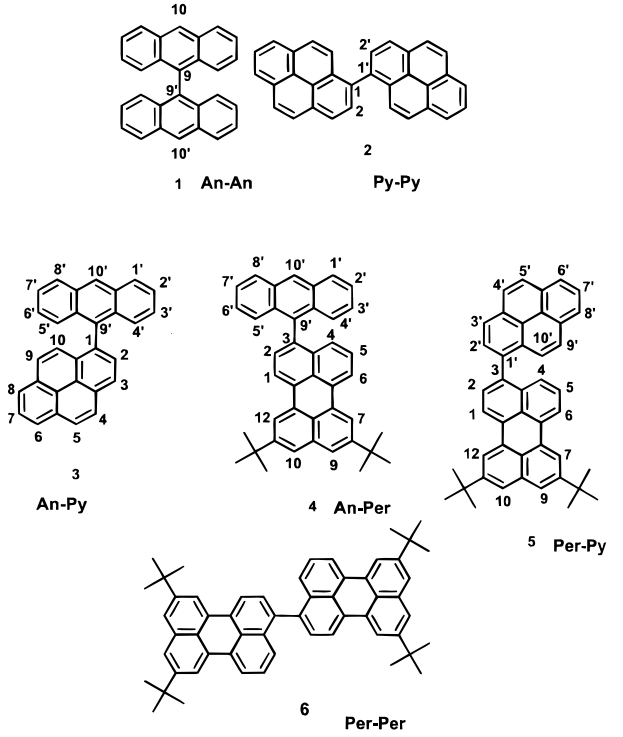

charge separation in the neutral species, which leads to oppositely charged monoradical subunits. This work therefore deals with the spectroscopic properties of different asymmetric biaryls (Scheme 1) and investigates if it is possible to predict the magnitude of the electronic coupling between the subunits.

2. Synthesis of Asymmetric Biaryls

The Pd(0)-catalyzed aryl−aryl cross-coupling according to Suzuki[17] can be used as a general procedure for the synthesis of asymmetric biaryls. The proposed route is examplified as outlined in Scheme 2, with the monobromo derivatives as starting material for the synthesis of 1-(9′-anthryl)pyrene (**3**). From the bromoanthryl, the boronic acid derivative of the lithiated intermediate is prepared and the final product results in high yield after Pd(0)-induced coupling and chromatographic separation. Compounds **4** and **5** are prepared in a similar manner. The detailed preparation procedures are described in sections 6.2, 6.3, and 6.4.

3. Results

3.1. Characterization of the Neutral Compounds by Cyclic Voltammetry and Optical Absorption. The cyclic voltammograms of 1-(9′-anthryl)pyrene (**3**), 3-(9′-anthryl)-8,11-di(*tert*-butyl)-perylene (**4**), and 3-(1′-pyrenyl)-8,11-di(*tert*-butyl)-perylene (**5**) demonstrate that the first two reduction potentials of each compound are reversible (Table 1), and it should be noted that the first reduction potentials of the three asymmetric compounds are very similar to those of the parent molecules anthracene, perylene, and pyrene, or their phenyl-substituted derivatives. Thus, there are negligible conjugative interactions and the biaryls consist of two electronically almost separated π-units. These findings are also reflected by the results of the UV/vis measurements (Table 2), since the spectra of the neutral dimers show only a small bathochromic shift compared to the model monomers and appear as superposition of the absorption

SCHEME 2: General Procedure for the Synthesis of Asymmetric Biaryls 3−5

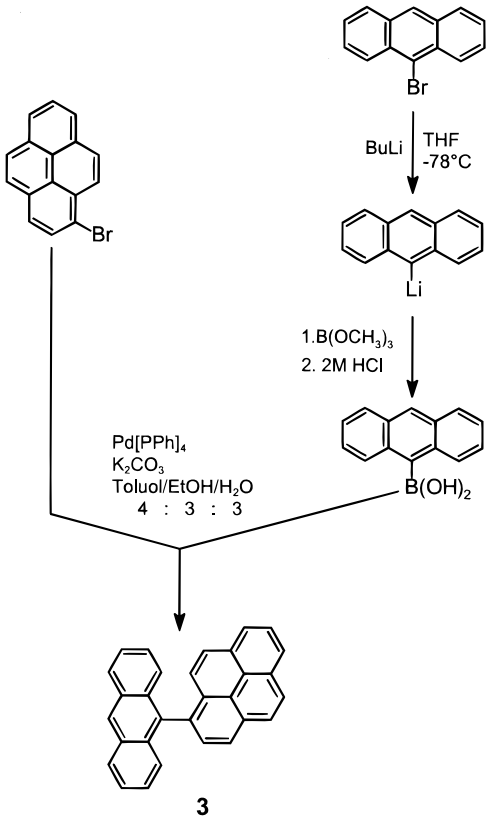

TABLE 1: Redox Potentials (vs SCE) of the Biaryls 3−5 Measured in THF with [TBA]PF_6 as Conducting Salt[a]

compound	$E^1_{1/2}$/V	$E^2_{1/2}$/V	$E^3_{1/2}$/V	$E^4_{1/2}$/V
3	−2.13	−2.30	−2.40	−2.85
4	−1.93	−2.22	−2.48	−2.73
5	−1.90	−2.18	−2.40	

[a] Ferrocene was used as an internal standard (310 mV vs SCE) for calibration.

TABLE 2: Optical Absorption of the Neutral Biaryls 3−5 in Comparison with the Parent Compounds Perylene, Anthracene, and Pyrene[a]

compound	$\lambda_{max,perylene\ unit}$ (nm)	$\lambda_{max,anthracene\ unit}$ (nm)	$\lambda_{max,pyrene\ unit}$ (nm)
3		386	340
4	444	383	
5	444		340
perylene	436		
anthracene		376	
pyrene			334

[a] All the experiments were performed in THF at room temperature.

spectra of the isolated chromophores. This points toward a hindered conjugation between the extended π-units.

3.2. Radicals in Solution. Reduction of the asymmetric biaryls **3**, **4**, and **5** with potassium in THF under high vacuum as well as oxidation by means of 2,3-dichloro-5,6-dicyanobenzoquinone (DDQ) or antimony pentachloride in dichloromethane yields strongly colored solutions of the charged ions, which were characterized by UV/vis and EPR/ENDOR spectroscopy in the same sample tube after one another at a given redox stage. Back and forth control of the two methods showed no further change of the generated species between the experiments and that the

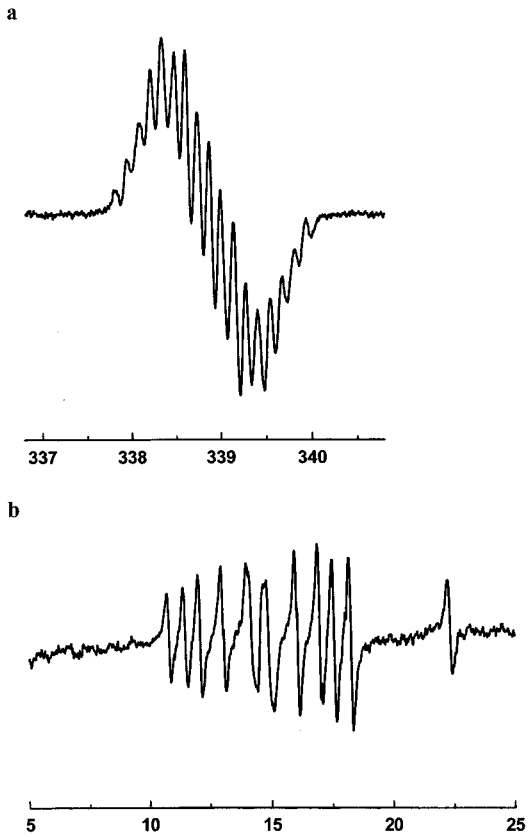

Figure 1. EPR (a) and ENDOR spectra (b) of monoanion $\mathbf{3}^{\bullet-}$ in THF solution at 240 K.

generated anionic species have a long lifetime (months). The identification of the different radical ions generated rests upon comparison with the well-established spectroscopic data of the parent compounds anthracene, perylene, and pyrene.

One question to deal with is whether the unpaired electron of the monoanions of the asymmetric biaryls is localized on one subunit or whether it is delocalized over both electrophoric units as can be observed in the case of the related symmetric biaryls 9,9′-bianthryl (**1**) and 1,1′-bipyrenyl (**2**). Another point of interest represents the possibility of the formation of biradicals in the doubly charged species (dication or dianions).

3.2.1. Monoanions and Monocations. The contact of a solution of 1-(9′-anthryl)pyrene (**3**) with a potassium mirror leads to the formation of the monoanion. The intensive EPR spectrum of $\mathbf{3}^-$ in solution (Figure 1) shows relatively high resolution, but the signals are too complex for an unambiguous interpretation. The ENDOR spectrum of $\mathbf{3}^-$, taken at a central saturated line of the EPR spectrum, yields much better resolution and exhibits seven pairs of lines yielding one large, four medium, and two small hyperfine coupling (hfc) constants (Table 3 and Figure 1). Since the redox potential of anthracene is slightly less negative than that of pyrene and the coupling constants of $\mathbf{3}^-$ are in good agreement with those of the monoanion of 9-phenylanthracene,[18] it is obvious that the unpaired electron is localized on the anthracene unit. Therefore, the largest hfc constant is assigned to the 10-position of anthryl and the other four smaller ones to the other four pairs of equivalent protons of the anthryl unit, while two very small coupling constants (0.024 and 0.010 mT) are derived from protons on pyrene but cannot be assigned properly to defined positions. To account for counterion influences, **3** was also charged electrochemically (THF, $TBAPF_6$) in a specially developed cell.[15c] The observed ENDOR spectra of the monoanions $\mathbf{3}^-$ were identical with those obtained upon chemical reduction.

The EPR spectrum of $\mathbf{4}^-$ shows eight sets of lines caused by the hyperfine interaction of the unpaired electron with seven hydrogen atoms at positions of high spin density (Figure 2). The corresponding ENDOR spectrum at 240 K consists of four large coupling constants. Computer simulation of the EPR spectrum allows an unambiguous assignment to the seven protons mentioned above (Table 3 and Figure 2). By comparison with the hfc constants of the monoanion of 3,3′-bis(8,11-di-(*tert*-butyl)perylenyl) (**6**), which has been investigated earlier,[19] it can be concluded that in this case the perylenyl unit is charged.

The treatment of **4** with small amounts of DDQ in dichloromethane leads to the formation of the stable monocation again localized on the perylene unit. The spectral width of the EPR spectrum of $\mathbf{4}^+$ is larger than that of the monoanion, which is caused by the slightly larger hfc constants at the peri positions of the perylenyl unit in the case of the cations.[22] The evaluation of the ENDOR spectrum of $\mathbf{4}^+$, pictured in Figure 2, leads to four hfc constants (Table 3), and the computer simulation with the given multiplicities is in good agreement with the experimental spectrum.

The reduction of **5** leads to the formation of the monoanion, which is again observable in the EPR spectrum by the appearance of eight broad lines. In contrast to $\mathbf{4}^-$, the ENDOR spectrum of $\mathbf{5}^-$ consists of an additional large coupling and shows that the odd electron is localized on the perylene unit and that the bay positions of perylene possess different spin densities. Table 3 shows the coupling constants determined from the ENDOR experiment. By using the given multiplicities, one obtains a good simulation of the experimental EPR spectrum (Figure 3).

The oxidation of **5** performed using DDQ and trifluoroacetic acid in dichloromethane at 240 K facilitates the formation of a monocation that is stable for about 70 min and enables the measurement of EPR and ENDOR spectra.

The ENDOR spectrum of $\mathbf{5}^+$ (Figure 3) reveals five large hfc constants corresponding to seven hydrogen atoms, similar to the results for the monoanion $\mathbf{5}^-$ (Table 3).

A different behavior of these three compounds is also discernible by comparing the optical absorptions of the monocharged species of the asymmetric biaryls (Figure 4). In the vis/IR spectrum of $\mathbf{3}^-$, an absorption typical of the substituted anthracene anion at 671 nm is observable, as well as a broad but very weak charge-transfer band in the NIR domain at around 1800 nm. For the other two monoanions $\mathbf{4}^-$ and $\mathbf{5}^-$, the same intensive absorption in the visible region at around 588 nm is observed, characteristic of the negatively charged perylene. This confirms the results and the assignments from the EPR/ENDOR measurements to the charged subspecies. In the vis/NIR spectrum of $\mathbf{5}^-$, an additional well-developed charge-transfer band appears at 1650 nm (Figure 4) while for $\mathbf{4}^-$ no IR absorption is found at all. Although the optical absorption spectra ($\sim 10^{-11}$ s) operate in a different time scale than the CW EPR spectra ($\sim 10^{-7}$ s), they give additional proof of the generated species. The indicated charge-transfer (CT) bands for $\mathbf{3}^-$ and $\mathbf{5}^-$ in the absorption, on the other hand, is not paralled by a fast exchange (delocalization) in the slower EPR regime, as is sometimes found for symmetric biaryls as $\mathbf{2}^-$.

The above results demonstrate that opposite to their symmetric counterparts the radical ions of the asymmetric biaryls **3**−**5** do not exhibit an electron self-exchange process at ambient temperatures leading to complete charge and spin delocalization

TABLE 3: Hyperfine Coupling Constants (HFCs) a_H and the Corresponding Number of Equivalent Protons of the Mono- and Triply Charged Species of Compounds 3−5 (Numbering According to Scheme 1)[c]

compounds and charged states	a_H/mT, (equiv protons), [assignment to molecular position where possible]
3, monoanion $\mathbf{3}^-$, $\mathbf{A}^{\bullet-}$Py	0.559, (1), [10′]; 0.266, (2), [4′,5′]; 0.217, (2), [1′,8′]; 0.172, (2), [2′,7′]; 0.109, (2), [3′,6′]; 0.024, 0.010, [Py[a]]
trianion $\mathbf{3}^{3-}$, $\mathbf{A}^{2-}$Py$^{\bullet-}$	0.475, (3), [3,6,8]; 0.289, (1); 0.219, (2); 0.132, (1); 0.100, (2)
4, monoanion $\mathbf{4}^-$, **A**−Per$^{\bullet-}$	0.335, (2), [peri[b]]; 0.315, (1), [peri[b]]; 0.304, (2), [bay[b]]; 0.272, (2), [bay[b]]; 0.019, (2)
monocation $\mathbf{4}^+$, **A**−Per$^{\bullet+}$	0.432, (2), [peri[b]]; 0.374, (1), [peri[b]], 0.287, (2), [bay[b]]; 0.272, (2), [bay[b]], 0.04, 0.01[a]
trianion $\mathbf{4}^{3-}$, $\mathbf{A}^{\bullet-}$Per^{2-}	0.475, (1), [10]; 0.290, (2), [1,8]; 0.271, (2), [4,5]; 0.158, (2); 0.139, (2)
5, monoanion $\mathbf{5}^-$, Py−Per$^{\bullet-}$	0.330, (2), [peri]; 0.321, (1), [peri]; 0.295, (2), [bay]; 0.250, (1), [bay]; 0.235, (1), [bay]; 0.04−0.02[a]
monocation 5^+, Py−Per$^{\bullet+}$	0.431, (1),[peri]; 0.403, (1), [peri]; 0.345, (1); 0.283, (2), [bay]; 0.262, (2), [bay]; 0.03 [a]
trianion $\mathbf{5}^{3-}$, Py$^{\bullet-}$Per^{2-}	0.460, (3), [3′, 6′, 8′]; 0.239, (2), 0.172, (1); 0.159, (1); 0.101, (1); 0.095, (1)

[a] Not further assigned. [b] Positions 4, 9, 10 called peri, and positions 1, 6, 7, 12 called bay of perylene (Scheme 1). [c] **A** = anthryl. Per = perylenyl. Py = propenyl. bay peri = assignment.

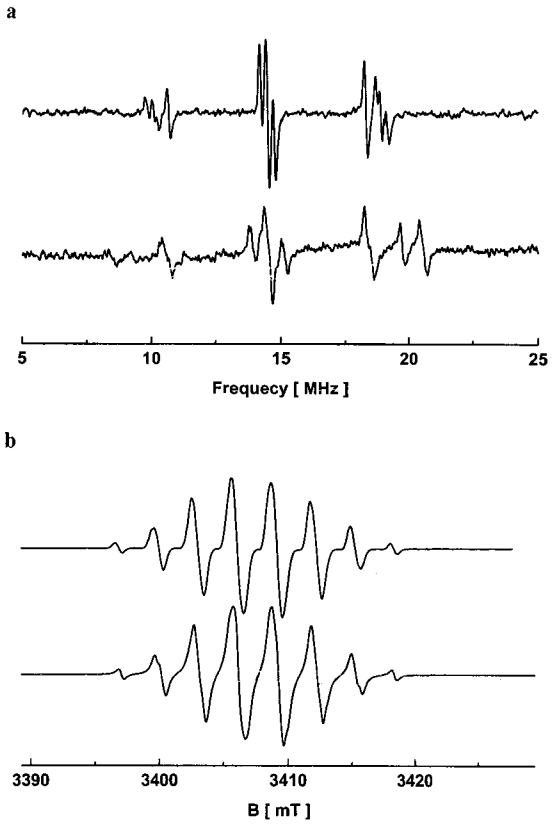

Figure 2. (a) ENDOR spectra of monoanion $\mathbf{4}^{\bullet-}$ (upper) and monocation $\mathbf{4}^{\bullet+}$ (lower spectra) in THF and dichloromethane solution, respectively, at 240 K and (b) EPR spectrum of the monoanion $\mathbf{4}^{\bullet-}$ at 240 K and the corresponding computer simulation.

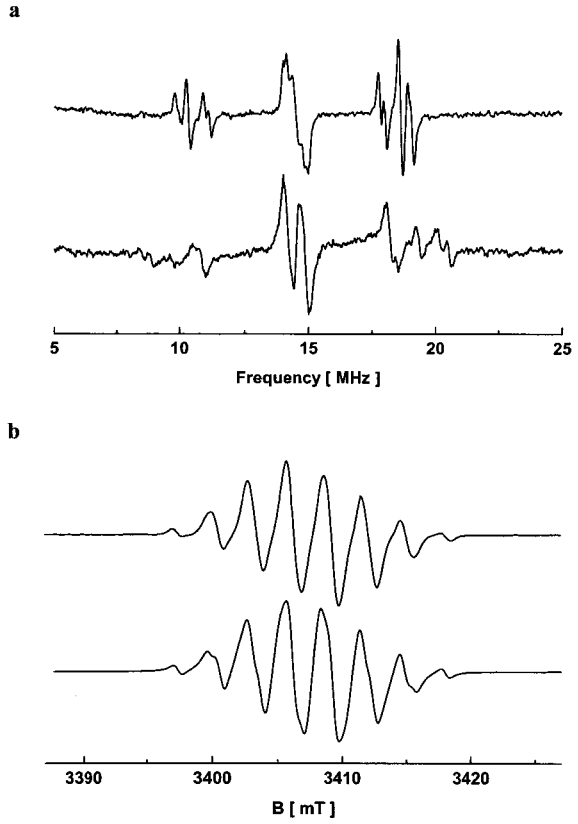

Figure 3. (a) ENDOR spectra of monoanion $\mathbf{5}^{\bullet-}$ and monocation $\mathbf{5}^{\bullet+}$ in THF solution at 240 K and (b) EPR spectrum of monoanion $\mathbf{5}^{\bullet-}$ at 240 K and the corresponding computer simulation.

over the dimers. Instead, charge and spin are localized, and the spin-carrying site is always given by the unit possessing the slightly lower reduction or oxidation potential.

3.2.2. Dianions and Dications. The dianions are easily formed upon further contact with the potassium mirror, while for the dications generally fresh samples were prepared, with a larger amount of suitable oxidant. As a first example, successive reduction of $\mathbf{3}^{\bullet-}$ is described, leading to a new paramagnetic species, with characteristic optical absorptions (Table 4) and an EPR spectrum of increasing intensity in liquid solution. This new species can be assigned to the biradical $\mathbf{3}^{2-}$.

Here, the doubly charged species possess two unpaired electrons either with parallel spins, corresponding to a triplet ground state, or with antiparallel spins in the case of a singlet ground state. For the characterization of spin−spin interaction one needs the spin Hamiltonian H_{Spin} for quantum numbers of the spin angular momentum S larger than $^1/_2$. H_{Spin} can be described in first order by the electronic Zeeman contribution H_{eZ} together with the fine structure contributions H_{SS} (eq 1) where higher order terms from hyperfine H_{hf}, nuclear Zeeman H_{nZ}, and quadrupole interactions H_Q have been neglected.[20,21]

$$H = H_{eZ} + H_{SS} + (H_{hf} + H_{nZ} + H_Q) = \beta B\mathbf{g}S + S\mathbf{D}S + \ldots \quad (1)$$

where **g** and **D** are 3 × 3 tensors and $\underline{B}$ and $\underline{S}$ are vectors.

The additional fine structure or zero-field splitting term $\underline{S}\mathbf{D}\underline{S}$ leads to characteristic further splittings of the (m_s) energy levels as given in eq 2.

$$\underline{S}\mathbf{D}\underline{S} = -(D_x S_x^2 + D_y S_y^2 + D_z S_z^2) \quad (2)$$

where D_x, D_y, and D_z are the eigenvalues of the fine structure tensor (D_z is the largest component in absolute value) and x, y, and z are the eigenvectors. Because of the traceless property of **D**, these three principal values can be reduced to two components,[21] called zero-field splitting (zfs) parameters, which have been denoted as $D = -(^3/_2)D_z$ and $E = (^1/_2)(D_x - D_y)$. They characterize the strength (D) and the symmetry (E) of the dipolar

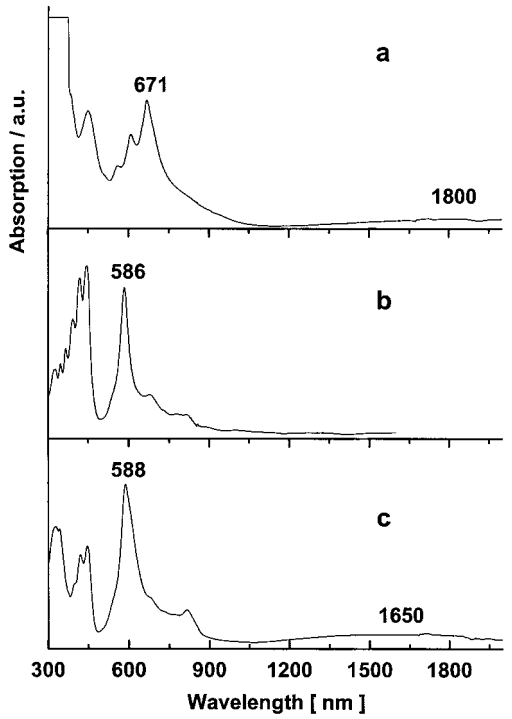

Figure 4. Vis/IR spectra at room temperature of the monoanions (a) $\mathbf{3}^-$, (b) $\mathbf{4}^-$, and (c) $\mathbf{5}^-$.

TABLE 4: Vis/NIR Optical Absorption Maxima of the Negatively Charged Species of the Biaryls 3−5 in THF at Room Temperature

	λ/nm		
compound	monoanions	dianions	trianions
3	452, 560, 609, 671, 1800[a]	452, 1300	491, 603, 723
4	586, 678, 822	454, 581, 690	
5	588, 815, 1650[b]	1400	388, 459, 501, 603

[a] Weak. [b] Strong.

interaction. It is convenient to express D and E in units of magnetic field (mT) by defining the quantities $D' = D/(g\beta)$ and $E' = E/(g\beta)$, where D' and E' are the experimental values determined from the magnetic field differences between the resonances. Since the dipolar components average to zero, the determination of D' and E' is only possible in anisotropic systems; i.e., the solutions of the radical ions have to be frozen.

The EPR spectrum of the frozen solution of $\mathbf{3}^{2-}$ consists of one central signal for the monoanion $\mathbf{3}^-$ and six symmetrically placed spectral peaks corresponding to the X, Y, and Z components of the biradical, which can be assigned to a triplet species with rhombic symmetry (Figure 5).[21]

Since the EPR spectral width is approximated by $2D'$,[20] D' was determined to be 16.1 mT. From the small splitting of the Y and X components, one can deduce the asymmetry parameter $E' = 1.8$ mT. The assignment is confirmed by the computer simulation of the triplet EPR spectrum (see Figure 5).

With the assumption of a point−dipole approximation (eq 3) an average mean distance of the radical sites $R = 0.56$ nm is found for $\mathbf{3}^2$:

$$D'\,[0.1\text{ mT}] \cong \frac{3g_e^2\beta^2}{4R^3} \qquad (3)$$

The $\Delta m_S = 2$ transition observed at the half-field resonance

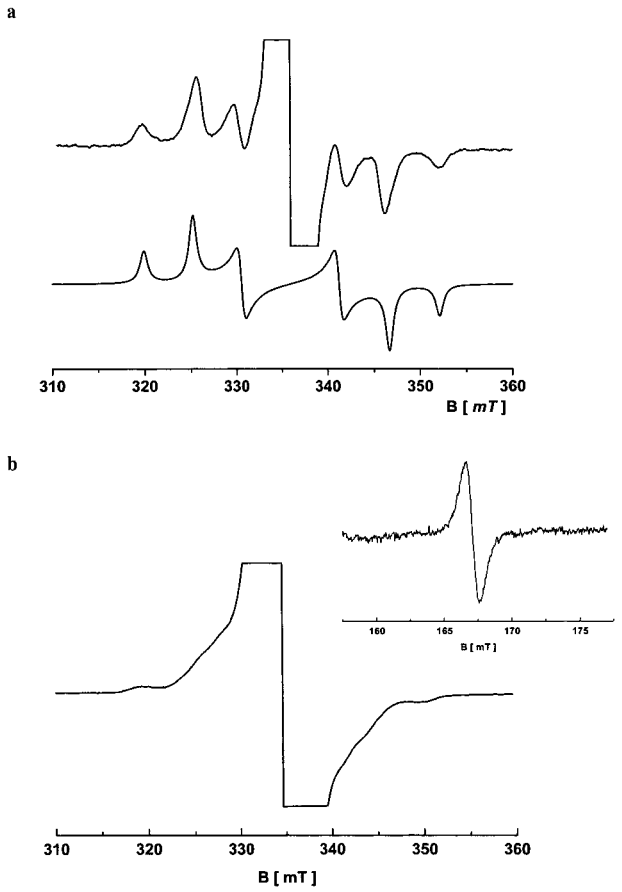

Figure 5. (a) EPR spectrum of the triplet state (only the $\Delta m_s = 1$ field region is shown) and the corresponding computer simulation of biradical $\mathbf{3}^{2,2-}$ in frozen THF/$2K^+$ solution (135 K). $|D'| = 16.1$ mT and $|E'| = 1.8$ mT are used for the simulation. (b) $\Delta m_S = 1$ field region of the EPR spectrum of dication $\mathbf{3}^{2+}$ in $CH_2Cl_2/SbCl_5$ solid state ($T =$ 130 K) and the corresponding $\Delta m_S = 2$ transition.

yields additional evidence that the detected species is in a triplet state at this temperature (135 K).

If the biradical $\mathbf{3}^{2+}$ is generated by oxidation with antimony pentachloride, the EPR spectrum in frozen solution again shows the typical structure for a triplet state with rhombic symmetry. The evaluation of the zfs parameter D' leads to 15.0 mT, but the asymmetry parameter E' is difficult to determine. The measured $\Delta m_S = 2$ transition further confirms the biradical nature of the dication (Figure 5).

The doubly charged species of **4** are characterized by UV−vis (Table 4) and EPR spectroscopy in liquid solution, respectively. The paramagnetic character of the dianion led to additional investigations in frozen solution. EPR measurements of the paramagnetic dianion $\mathbf{4}^{2-}$ at 135 K in THF delivers a spectrum with six lines symmetrically placed with respect to the Zeeman resonance (e.g., the signal of the monoanion $\mathbf{4}^-$) belonging to a triplet state with rhombic symmetry, since $D_x \neq D_y$ (Figure 6). The evaluation of the six signals of the $\Delta m_S =$ 1 field region yields the zfs parameters $D' = 12.4$ mT and $E' =$ 0.7 mT, as well as the average distance between the interacting spin centers of $R = 0.61$ nm, which is slightly larger than for $\mathbf{3}^{2-}$ and indicates a weaker dipole interaction. The temperature dependence of the signal intensities in the range 10−80 K reveals a thermally activated triplet state, with maximum intensity around 30 K, corresponding to ΔE_{ST} of about 90 cal/mol (375 J/mol). In comparison with earlier findings for $\mathbf{1}^{2-}$ ($\Delta E_{ST} = 60$ cal/mol)[5] and 2,2′-bipyrenyl ($\Delta E_{ST} = 120$ cal/mol

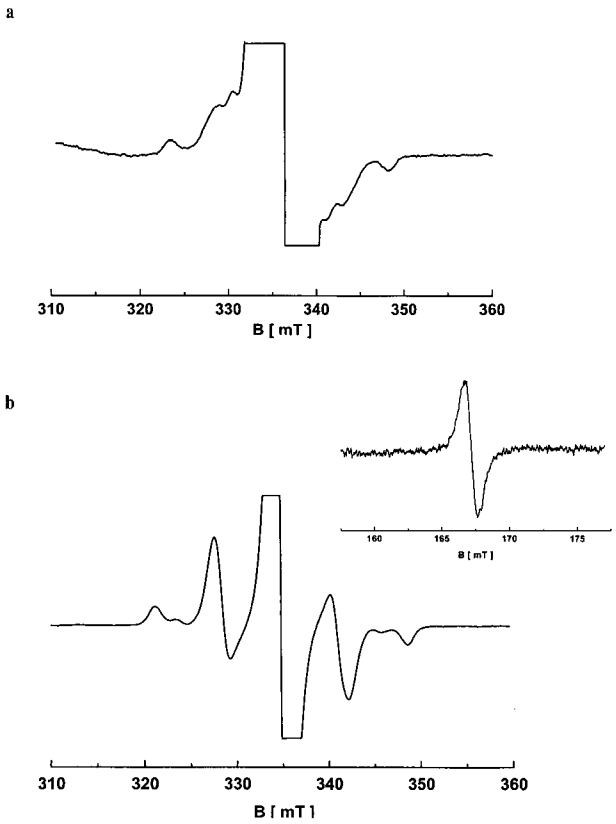

Figure 6. (a) EPR spectrum (only the $\Delta m_s = 1$ field region) of biradical $\mathbf{4}^{2\bullet 2-}$ in frozen THF/$2K^+$ solution. (b) $\Delta m_S = 1$ field region of the EPR spectrum of dication $\mathbf{4}^{2\bullet 2+}$ in frozen $CH_2Cl_2/SbCl_5$ (130 K) and the corresponding $\Delta m_S = 2$ transition in the inset.

(0.5 kJ/mol))[8] the stability of the triplet state of $\mathbf{4}^{2-}$ is intermediate.

The triplet state is also accessible by a quick oxidation of **4** with antimony pentachloride under anaerobic conditions. The EPR spectrum of $\mathbf{4}^{2+}$ in frozen solution (135 K) reveals a central signal assigned to the monocation and four additional resonances that can be assigned to a triplet state with nearly axial symmetry (Figure 6). A slightly larger zero-field splitting ($D' = 13.7$ mT) for the dication is found compared to the dianion because of the larger spin density at the bridgehead positions.[22]

In contrast to the increased paramagnetic contributions in the case of the dianions and dications of **3** and **4**, further charging of **5** leads to a decrease of the paramagnetic contributions, and the doubly charged species $\mathbf{5}^{2-}$ and $\mathbf{5}^{2+}$ are diamagnetic. The UV−vis spectra recorded for these species represent another useful reference for identifying the intact dianion, since the distinct absorptions of perylene and pyrene anions are still present together with a hypsochromically shifted IR band (Table 4).

3.2.3. Trianions. The triply charged species were only accessible through anionic charging, while cationic charging ended with the formation of doubly charged states. The spectroscopic evidence of the formation of trianions are again provided by UV−vis and EPR measurements. Successive reduction of the dianion of **3** reveals a drastic change in the EPR and visible spectra at room temperature, already indicating the formation of the trianion. From the ENDOR spectrum of $\mathbf{3}^{3-}$, one can extract six hfc constants (Table 3), and the multiplicity and size of the largest five constants leads to the conclusion that the unpaired electron is localized on the pyrene unit with a minor amount of spin density being distributed into the anthryl unit, indicated by a small hfc constant (0.010 mT) that cannot be assigned safely to molecular positions.

By continuing the reduction of $\mathbf{4}^{2-}$, the shape of the EPR spectrum at room temperature changes and six hfc constants can be determined from the corresponding ENDOR experiment. The values of the hfc constants for $\mathbf{4}^{3-}$ as summarized in Table 3 lead to the conclusion that the unpaired electron is probably localized on the anthracene unit, although the size of the largest coupling constant is smaller (0.475 instead of 0.540 mT) than for a singly charged substituted anthracene as in $\mathbf{1}^-$ or $\mathbf{3}^-$. The computer simulation of the resolved EPR spectrum confirms this assignment and the conclusion that the unpaired electron is localized on the anthracene unit.

Also further reduction of the diamagnetic dianion of **5** leads to the formation of a new paramagnetic species. Six hyperfine coupling constants are detected by means of ENDOR spectroscopy, and the largest one is on the order of the largest hfc constant of a monocharged pyrene (Table 3). It follows that two negative charges reside on the perylene unit, whereas the third unpaired electron is localized on the pyrene unit. The comparison with a monocharged pyrene allows the assignment of the coupling constants to different positions within the pyrene unit and results in a good simulation of the experimental EPR spectrum.

4. Discussion and Comparison to Photophysical Properties

4.1. Ground-State Properties of the Ions. The investigations of the monoanions of the asymmetric biaryl compounds demonstrate that no ion exchange processes take place and that the unpaired electron is always located on the π subunit with the lower redox potential, the perylene unit in the case of $\mathbf{4}^-$ and $\mathbf{5}^-$ and the anthrylene unit in the case of $\mathbf{3}^-$. The same behavior has been found for the monocations $\mathbf{4}^+$ and $\mathbf{5}^+$, where the unpaired electron is located on the perylene subunit that possesses the lower oxidation potential. This is contrary to the findings for monoanions of symmetric biaryls, e.g., of $\mathbf{1}^-$ and $\mathbf{2}^-$, where a complete delocalization of charge and spin density, at least at the beginning of the reduction, has been observed experimentally. The results for **3**−**5** are in good agreement with the corresponding AM1 calculations, where the HOMO and LUMO are also located on the π-subunit with the lower redox potential. Thus, the monocharged biaryls **3**−**5** are comparable with phenyl- or 2-methylphenyl-substituted π-systems where just a small amount of spin density is transferred into the second aryl. While often phenyl hyperconjugation[18] has been used to explain the spreading of spin density in phenyl-substituted aromatics, we may speak more generally of aryl hyperconjugation in the case of asymmetric biaryls.[23]

An essential difference between the asymmetric compounds can be shown by the comparison of the corresponding optical absorption spectra (Figure 4). The Vis/NIR spectrum of $\mathbf{5}^-$ exhibits a fairly intense absorption in the NIR region (1650 nm) characteristic of a charge-transfer band. Also for $\mathbf{3}^-$, a NIR band at around 1800 nm is found, but its intensity is weak, and for $\mathbf{4}^-$ no band in the NIR region could be found. Because of the reduced steric hindrance caused by the interactions of the hydrogen atoms between the subunits of **5,** the equilibrium twist angle ($\theta \cong 70°$, AM1) is lower than for **3** ($\theta \cong 90°$, AM1) and **4** ($\theta \cong 90°$, AM1) and one can correlate the appearance of the strong NIR absorption for $\mathbf{5}^-$ with the better overlap of the π-orbitals (Figure 4).

Indeed, a simple description of the wave function of the CT state by eq 4 is able to relate the intensity of the CT band with

the coupling matrix element V between ground-state GS and zero-order electron-transfer state ET(0).

$$\Psi_{CT} = a\Psi_{ET(0)} + b\Psi_{GS} + c\Psi_{LE} \quad (4)$$

The admixture of locally excited (LE) states is important for CT states of neutral species that are situated energetically close to the LE states in the vis/UV region.[24] In the case of the radicals studied here with very low-lying CT states that are far apart from the LE states, the contribution of LE to the total wave function of the CT state can be neglected ($c \approx 0$). Following Verhoeven et al.[25] in this case the absolute intensity or transition moment f of the CT band is directly determined by the coupling matrix element V:

$$f = 10^{-5}\mu^2V^2/\nu \quad (5)$$

In this case, μ and ν are the dipole moment and energy of the CT state, respectively. V, on the other hand, is related to the coupling of CT to the ground state, i.e., to the overlap of the π-orbitals of the donor and acceptor moieties. For a perpendicular arrangement of donor and acceptor (D and A), $V = 0$ and the HOMO and LUMO of the combined system are localized on D and A, respectively. For $\theta \neq 90°$, these orbitals mix, and we can write for the general case

$$\psi_{HOMO} = (1 - \lambda_H)\psi_{HOMO(D)} + \lambda_H\psi_{HOMO(A)} \quad (6)$$

$$\psi_{LUMO} = \lambda_L\psi_{LUMO(D)} + (1 - \lambda_L)\psi_{LUMO(A)} \quad (7)$$

where only the most important mixing of pairs of energetically close-lying orbitals has been considered.

At 90°, where $V = \lambda_L = \lambda_H = b = 0$, optical excitation from HOMO to LUMO leads to the pure one-electron ET(0) state

$$\Psi_{CT} = \Psi_{ET(0)} \quad (8)$$

The transition moment is then given by eq 9,

$$M_{CT}(\theta{=}90) = \langle\psi_{GS}|er|\psi_{ET(0)}\rangle = \langle\psi_{HOMO(D)}|er|\psi_{LUMO(A)}\rangle = 0 \quad (9)$$

due to the vanishing overlap between $\psi_{HOMO(D)}$ and $\psi_{LUMO(A)}$.

For $\theta \neq 90°$, λ_H and λ_L differ from 0, and M_{CT} is then nonzero because of the admixture of ground and possibly locally excited states. The twist angle θ can in principle be determined from the oscillator strength by eq 5 if the usual angular dependence $V = V(0) \cos\theta$ is assumed. However, because of the unknown concentration of the ions studied, it was not possible to determine the oscillator strengths quantitatively.

4.2. Excited-State Properties of the Neutral Species. To find a possible relation between the formation of paramagnetic biradicals for the doubly charged species in the ground state and the formation of charge-transfer type biradical excited states for the uncharged asymmetric biaryls, photophysical experiments were carried out. For this reason, the solvent polarity dependence of the fluorescence spectra and that of the photophysical rate constants were determined. Bianthryl (**1**) has been thoroughly studied in this context, and the solvent-induced excited-state charge separation, accompanied in this symmetric case by a symmetry-breaking process,[26] manifests itself (i) by a solvatochromic red shift of the fluorescence spectra[27−30,32] and (ii) by a reduction of the rate constant k_f of the emissive transition[29,30] explainable by the near-perpendicular arrangement of the subunits in the charge-transfer (CT) excited state[26,32] as well as in the ground state.[34] In other symmetric systems such as bipyrenyl **2** and biperylenyl **6**, these effects were predicted[34b] to be weaker, and this was tentatively correlated with the smaller steric hindrance and therefore less perpendicular ground-state structure compared to **1**.[33]

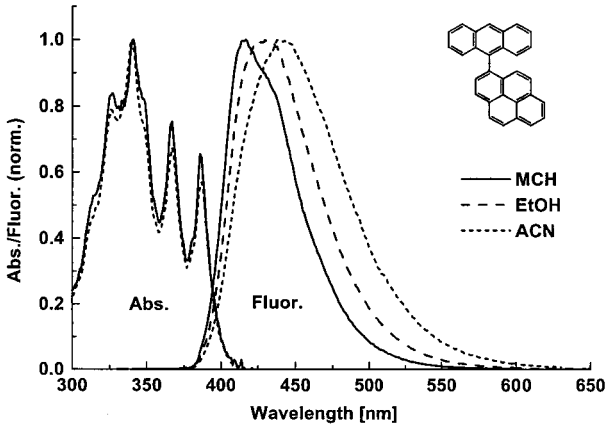

Figure 7. Normalized absorption and fluorescence spectra of **3** in solvents of different polarity at room temperature (MCH, methylcyclohexane; EtOH, ethanol; ACN, acetonitrile).

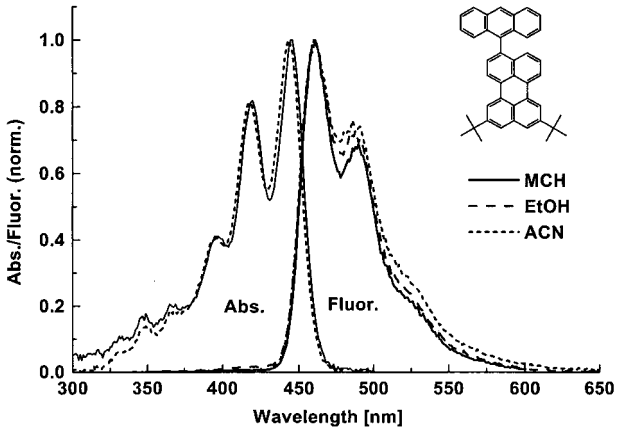

Figure 8. Normalized absorption and fluorescence spectra of **4** in solvents of different polarity at room temperature (MCH, methylcyclohexane; EtOH, ethanol; ACN, acetonitrile).

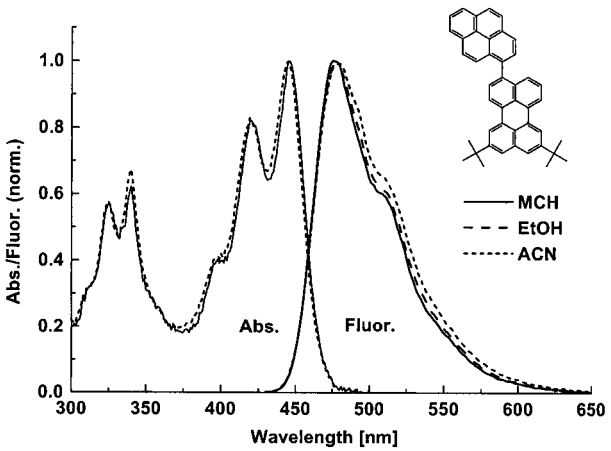

Figure 9. Normalized absorption and fluorescence spectra of **5** in solvents of different polarity at room temperature (MCH, methylcyclohexane; EtOH, ethanol; ACN, acetonitrile).

The absorption and fluorescence spectra for **3**−**5** as recorded in solvents of different polarity are shown in Figures 7−9. Only in the case of **3** a sizable solvatochromic red shift with increasing solvent polarity is observed, while the spectra shift very little to the red in the case of **4**. A solvatochromic red shift is

TABLE 5: Photophysical Properties of 3−5 in Solvents of Different Polarity at Room Temperature

compound/solvent	Φ_f	τ_f/ns	$k_f/10^7$ s^{-1}	$k_{nr}/10^7$ s^{-1}	M_f [D]
3/methylcyclohexane	0.71	3.7	19	7.9	4.5
3/ethanol	0.70	4.9	14	6.1	4.0
3/acetonitrile	0.58	6.0	10	7.0	3.6
4/methylcyclohexane	0.73	3.3	22	8.4	5.6
4/ethanol	0.79	3.7	22	5.8	5.6
4/acetonitrile	0.64	4.2	15	8.6	4.9
5/methylcyclohexane	0.64	2.7	24	14	6.1
5/ethanol	0.68	2.9	23	11	6.1
5/acetonitrile	0.64	2.9	22	13	6.1

completely absent for **5**. If the wave function of the emitting state is assumed to be a superposition of a nonpolar locally excited (LE) and a strongly polar charge transfer (CT) contribution,[35] then the different solvent dependence of the fluorescence spectra can be interpreted by different weights of charge-transfer contributions to the total fluorescence spectrum. By use of the fluorescence quantum yields and lifetimes, the rate constants of the emissive (k_f) and nonemissive (k_{nr}) excited-state decay as well as the transition moment for fluorescence decay of the excited state (M_f) can be determined using eq 10 (Table 5).[34c] The data for **3** and **4** demonstrate that the radiative decay rate constant k_f and the transition moment M_f decrease with increasing solvent polarity, consistent with an increased CT contribution in polar solvents, whereas the nonradiative decay rate constant is more or less independent of solvent polarity in all cases. In contrast to **3** and **4**, the results for **5** show a solvent-polarity independent behavior for both radiative and nonradiative decay rate constants as well as for the transition moment M_f, indicative that CT contributions are absent.

$$k_f = \frac{64\pi^4}{3h} n^3 \bar{\nu}_f^3 M_f^2 \qquad (10)$$

The photophysical results suggest that the emitting excited state of **3** and **4** possesses some charge-transfer character, the contribution of which depends on the solvent polarity. Although only **3** reveals a solvatochromic shift in the fluorescence spectra, the decreasing transition moments for fluorescence M_f in both **3** and **4** indicate that also in the case of **4** a contribution from a state with less allowed and more polar character is observable in high-polarity solvents. Since the fluorescence decays observed are strictly monoexponential on the time scale used ($\geq$0.1 ns), we can infer either that a rapid excited-state equilibrium between an allowed, polarity-independent LE state and a solvent-sensitive less allowed CT state is established within times less than 0.1 ns or that the wave function of the emissive state is a true, vibronically induced mixture of LE and CT contributions with increasing weight of CT for highly polar solvents. Since **5** does not exhibit a decrease of k_f and M_f, the CT contribution for this compound is obviously absent, and the excited state can be better described by the LE contribution alone with both unpaired electrons residing on the same fragment (perylene) and a stronger electronic interaction between them compared to the CT state of **3** and **4**, where the two unpaired electrons reside on different moieties. These results are directly comparable with the results from EPR spectroscopy of the doubly charged ground-state species, i.e., CT contributions leading to partial charge separation as ($D^{\bullet+}A^{\bullet-}$) are only found in those molecules that are able to form biradicals ($D^{\bullet-}A^{\bullet-}$ or $D^{\bullet+}A^{\bullet+}$) upon doubly charging.

5. Conclusions

In summary, it has been found that ground- and excited-state properties show a strikingly parallel behavior with two odd electrons separated on different moieties for S_1(**3**,**4**) and S_0(**3**$^{2-}$,**4**$^{2-}$) but with the two odd electrons being spin-paired on the same moiety for S_1(**5**) and S_0(**5**$^{2-}$).

The following characteristic differences can be extracted from the EPR, ENDOR, UV, and fluorescence spectroscopic data of the asymmetric biaryls **3**−**5**.

(1) So far, only in symmetric biaryls a delocalization of the ground-state spin density over the complete molecule could be found, while asymmetric biaryls tend to localize the spin density on one subunit with some small transfer of spin density into the other unit (aryl hyperconjugation).

(2) Only the monoanions of **5** show an intense NIR absorption band (Table 4) that can be assigned to a charge-transfer transition, while it is very weak for **3**$^-$.

(3) Further charging of the monoradicals leads to the formation of paramagnetic biradicals in the case of **3** and **4**, while the doubly charged biaryl **5** is diamagnetic.

(4) The excited states of the neutral species can also exhibit charge separation linked with "electronic decoupling". In parallel with charge separation in the excited states observed for **3** and **4**, the dianions of **3** and **4** are found to be paramagnetic, whereas **5** shows diamagnetic behavior compared with that in the absence of excited-state charge separation.

From these characteristics, it is possible to classify the symmetric and asymmetric biaryls into weakly and medium strongly electronically coupled compounds. A strong coupling leads to the formation of a diamagnetic dianion or dication (**5**) without charge separation in the excited state (**5**), while a weak coupling between the subunits results in the formation of diionic or uncharged biradicals (**3**, **4**), where the subunits carry either the same charge (in the ionic ground-state species) or opposite charges (in the charge-separated excited state of the neutral species).

ESR/ENDOR measurements on mono- and dianions or -cations of **3**−**5** yield evidence that the (odd) electron in the monoradicals is localized on the moiety with the highest HOMO (for cation radicals) or with the lowest LUMO energy (anion radicals). In the doubly charged species (both dianion and dication), either diamagnetic spin-paired ground states are formed or paramagnetic biradicals with uncoupled spins (one electron or hole on each moiety) can occur.

The interaction between the two subunits is determined by the magnitude of the MO coefficients of the carbon centers at the bridgehead position and by the twist angle resulting from the steric hindrance.

By means of the McConnell equation[36]

$$a_H = Q\rho(x) \qquad (11)$$

the spin density ρ and thus the corresponding MO coefficients can be extracted from the measured coupling constants a_H. Starting from the well-investigated aromatic π-systems anthracene, perylene, and pyrene[37] and with the assumption that the connection of these molecules to form a biaryl does not dramatically change the magnitude of spin density, it is possible to compare the experimental results with theoretical data.

Table 6 shows that the expression consisting of the MO coefficients of the bridgehead carbon atoms ρ_i and the dihedral angle θ (AM1 calculation) as $\rho_1\rho_2 \cos(\theta)$ immediately allows a classification of biaryls **1**−**6**. The data of Table 6 are in accord with the experimental results of the symmetric and asymmetric biaryls and subdivide the compounds into weakly coupled systems (**1**, **3**, and **4)** and into more strongy coupled ones (**2** and **5)** based on spin densities and dihedral angle. The expression $\rho_1\rho_2 \cos(\theta)$ can thus be used to quantify the

TABLE 6: Calculated Spin Densities and MO Coefficients of the Carbon Centers at the Bridgehead by Position Determined by Using the Experimental Coupling Constants of the Monoradicals of the Parent Compounds Anthracene, Perylene, and Pyrene as Well as the McConnell Equation (See Text)

	θ (deg)	a_{H1} (mT)	a_{H2} (mT)	ρ_1	ρ_2	$\rho_1\rho_2 \cos(\theta)$
1	88	0.534	0.534	0.227	0.227	0.0009
2	70	0.475	0.475	0.202	0.202	0.0139
3	88	0.534	0.475	0.227	0.202	0.0008
4	88	0.534	0.353	0.227	0.150	0.0006
5	70	0.475	0.353	0.202	0.150	0.0103
6	70	0.353	0.353	0.150	0.150	0.0077

magnitude of the electronic coupling between the two subunits of a biaryl and allows us to make theoretical predictions about the electronic properties of biaryls and their corresponding oligomers. It is also possible to use calculated spin densities or MO coefficients.

The electronic decoupling behavior of **1**, **3**, and **4** in ground and excited states is related to the formation of high-spin states in compounds with more than two aryl units. Examples are known in the series of oligoanthrylenes where both high-spin states[5] and giant excited-state dipole moments[38] were detected. A general strategy for the development of such compounds is, according to the above considerations, to use weakly coupled systems.

The molecules studied here can also serve as a guideline for the development of new extended π-systems with electric field or light-induced switching properties[39] desirable for molecular electronic devices.

6. Experimental Section

6.1. Instrumentation and Methods. ^{1}H and ^{13}C NMR spectra were recorded on a Bruker AMX 500 spectrometer. Mass spectra were obtained on a FD-MS, VG-Instruments ZAB-2 mass spectrometer. Melting points were measured on a Büchi Dr. Tottolie apparatus (uncorrected). Elemental analyses were determined by the Department of Chemistry and Pharmacy of the University of Mainz. Column chromatography was performed employing a glass column packed with silica gel (70−320 mesh) with *n*-pentane as eluant. The commercial solvents were purified according to standard procedures.

The anions described here were prepared under high vacuum in tetrahydrofuran (THF) by contact with a potassium mirror in sealed quartz tubes with two side chambers. The cations were prepared in quartz sample tubes under argon in freshly distilled air and oxygen-free dichloromethane by means of 2,3-dichloro-5,6-dicyanobenzoquinone (DDQ) or antimony pentachloride. To account for counterion influences, anthrylpyrene (**3**) was also charged electrochemically in a specially developed cell.[15b,c] The observed ENDOR spectra of the monoanions $\mathbf{3}^-$ were identical with those obtained upon chemical reduction.

The EPR and ENDOR spectra were recorded on Bruker ESP 300 and ESP 300 E spectrometers at X-band (9.4 GHz) with 100 (EPR cavity) and 12.5 (ENDOR cavity) kHz modulation frequency. The temperature was controlled by a Bruker continuous flow N_2 cryostat and the very low temperature by an Oxford ESR 910 helium continuous flow cryostat.

The computer program for the simulation of biradicals has been written by Dr. Stoyan Karabunarliev for arbitrary spin states ($S = 0.5-5.5$) and direct diagonalization of the spin Hamiltonian.

Cyclic voltammograms were measured with a Princeton Applied Research model PAR 272, and ferrocene was used as an internal standard for calibration.

The optical absorption measurements were performed at ambient temperature in a quartz tube using a special sample holder and typical transmission detection with a Perkin-Elmer Lambda 9 spectrometer.

Quantum-corrected fluorescence spectra (concentrations less than 10^{-4} mol/L) were measured on an SLM-Aminco Bowman 2 fluorometer. Fluorescence quantum yields were determined relative to a solution of quinine bisulfate in 0.1 N H_2SO_4 ($\phi_f = 0.52$)[40] and corrected for the refractive index of the solvents. Decay times of aerated solutions were determined with the time-correlated single photon counting (SPC) technique[41] using equipment described elsewhere.[42] Synchrotron radiation from the Berlin electron storage ring BESSY operating in the single bunch mode was used for excitation.[42] The excitation wavelength was adjusted to the longest wavelength absorption band.

6.2. Synthesis of 1-(9-Anthryl)pyrene (3). An amount of 1.5 mL *n*-butyllithium (1.6 M/hexane) was added to a stirred solution of 0.6 g (2.13 mmol) of 1-bromopyrene in THF at −78 °C. After 15 min the temperature was increased to 0 °C followed by the addition of 0.24 mL of boronic acid trimethyl ester, which results in the formation of the 1-pyrenylboronic acid. After 20 min of stirring, the mixture was quenched with 0.01 M HCl. The solvent was removed under reduced pressure, and the residue was recrystallized from water and dried. An amount of 195 mg (0.79 mmol) of 1-pyrenylboronic acid was dissolved in ethanol and added to a mixture of 10 mmol of sodium carbonate in 20 mL of water and 204 mg (0.79 mmol) of 9-bromoanthracene in 40 mL of toluene. After addition of 40 mg of tetrakis(triphenylphosphine)palladium(0), degassing of the solution, and the exclusion of light, the mixture was heated at 115 °C for 30 h. Then the solvent was evaporated under reduced pressure and the crude product was purified by column chromatography (silica gel/*n*-pentane), which results in a yield of 65% of **3**.

^{1}H NMR (500 MHz, $CDCl_3$), δ: 8.58 (s, 1H, H_{10}); 8.32 (d, ^3J(H, H) = 7.7 Hz, 1H), 7.98 (d, ^3J(H, H) = 7.6 Hz, 1H); (H_{16}, H_{17} o. H_{18}, H_{19} o. H_{23}, H_{24}); 8.18 (d, ^3J(H, H) = 8.0 Hz, 1H), 8.04 (d, ^3J(H, H) = 7.5 Hz, 1H); (H_{20}, H_{22}); 8.13 (d, ^3J(H, H) = 9.2 Hz, 1H), 8.13 (d, ^3J(H, H) = 9.1 Hz, 1H); (H_{16}, H_{17} o. H_{18}, H_{19} o. H_{23}, H_{24}); 8.07 (d, ^3J(H, H) = 8.8 Hz, 2H), 7.30 (d, ^3J(H, H) = 9.0 Hz, 2H); (H_4, H_5, H_1, H_8); 7.94 (dd, $^3J_1$(H, H) = 7.9 Hz, $^3J_2$(H, H) = 7.6 Hz, 1H); (H_{21}); 7.72 (d, ^3J(H, H) = 9.2 Hz, 1H), 7.27 (d, ^3J(H, H) = 9.2 Hz, 1H); (H_{16}, H_{17} o. H_{18}, H_{19} o. H_{23}, H_{24}); 7.39 (dd, $^3J_1$(H, H) = 7.5 Hz, $^3J_2$(H, H) = 7.4 Hz, 2H), 7.15 (dd, $^3J_1$(H, H) = 7.6 Hz, $^3J_2$(H, H) = 7.4 Hz, 2H); (H_6, H_3, H_7, H_2). ^{13}C NMR (500 MHz, $CDCl_3$), δ: 135.4, 134.0 (C_9, C_{15}); 125.0, 124.9 (C_{27}, C_{29}); 131.6, 131.5, 131.4, 131.2, 131.1, 130.8 (C_{11}, C_{12}, C_{13}, C_{14}, C_{25}, C_{26}, C_{28}, C_{30}); 128.5, 127.1, 125.7, 125.3 (C_1, C_8, C_2, C_7, C_3, C_6, C_4, C_5); 129.4, 127.8, 127.7, 127.6, 127.1, 126.2, 125.8, 125.3, 125.2, 124.7 (C_{10}, C_{16}, C_{17}, C_{18}, C_{19}, C_{20}, C_{21}, C_{22}, C_{23}, C_{24}). FD-MS: *m*/*e* 378 (100, M^+). Anal. Calcd for $C_{30}H_{18}$: C, 95.20; H, 4.80. Found: C, 94.71; H, 4.98.

6.3. Synthesis of 3-(9-Anthryl)-8,11-di(*tert*-butyl)perylene (4). An amount of 2.7 mL of *n*-butyllithium (1.6 M/hexane) was added to a solution of 1 g (3.90 mmol) of 9-bromoanthracene in tetrahydrofuran at −78 °C. After 15 min, the reaction mixture was stirrred at 0 °C for 5 min. Then 0.44 mL of boronic acid trimethyl ester was added to the solution to form the 9-anthrylboronic acid. After 20 min, the mixture was quenched with 0.01 M HCl. After the solvent was evaporated under reduced pressure, the crude product was purified by recrystallization from water. An amount of 100 mg (0.45 mol) of the 9-anthrylboronic acid obtained was dissolved in 20 mL

of ethanol and added to a mixture of 10 mmol of sodium carbonate in 20 mL of water and 200 mg (0.45 mmol) of 3-bromo-8,11-di(*tert*-butyl)perylene in toluene. The last compound was prepared by methods analogous to those already described earlier.[19] After the addition of 40 mg of tetrakis-(triphenylphosphine)palladium(0), degassing of the solution with argon, and exclusion of light, the reaction mixture was heated to 115 °C for 30 h. After removal of the solvent under reduced pressure, the resulting residue was chromatographed on silica gel (*n*-pentane) to obtain 0.194 g of **4** in 80% yield.

^{1}H NMR (500 MHz, $CDCl_3$), δ: 1.45 (s, 9H), 1.43 (s, 9H); ($3H_{23}$, $3H_{24}$, $3H_{25}$ o. $3H_{28}$, $3H_{29}$, $3H_{30}$); 8.51 (s, 1H; H_{10}); 8.32 (s, 1H), 8.23 (s, 1H); (H_{18} o. H_{19}); 7.64 (s, 1H), 7.62 (s, 1H); (H_{17} o. H_{20}); 8.36 (d, ^3J(H, H) = 7.6 Hz, 1H), 7.46 (d, ^3J(H, H) = 7.6 Hz, 1H); (H_{11} o. H_{12}); 8.15 (d, ^3J(H, H) = 7.4 Hz, 1H), 6.85 (d, ^3J(H, H) = 8.3 Hz, 1H); (H_6 o. H_8); 8.02 (d, ^3J(H, H) = 8.5 Hz, 2H), 7.49 (d, ^3J(H, H) = 8.8 Hz, 2H); (H_5, H_4 o. H_8, H_1); 7.39 (dd, $^3J_1$(H, H) = 7.2 Hz, $^3J_2$(H, H) = 7.5 Hz, 2H), 7.21 (dd, $^3J_1$(H, H) = 7.6 Hz, $^3J_2$(H, H) = 7.7 Hz, 2H); (H_3, H_6 o. H_2, H_7); 7.12 (dd, $^3J_1$(H, H) = 7.9 Hz, $^3J_2$(H, H) = 7.8 Hz, 1H); (H_{15}). ^{13}C NMR (500 MHz, $CDCl_3$), δ: 26.0, 26.1 (C_{23}, C_{24}, C_{25}, C_{28}, C_{29}, C_{30}); 119.9, 120.3, 121.6, 123,1 (C_1, C_8, C_2, C_7, C_3, C_6, C_4, C_5); 113.1, 113.2, 114.3, 114.7, 118.2, 118.3, 121.0, 121.4, 124.4, 124.5 (C_{10}, C_{11}, C_{12}, C_{14}, C_{15}, C_{16}, C_{17}, C_{18}, C_{19}, C_{20}); 29.6, 29.7 (C_{22}, C_{27}); 125.6, 126.2 (C_{39}, C_{41}, C_{40}, C_{42}); 143.9 (C_{13}, C_9); 120.1, 124.1 (C_{32}, C_{37}); 125.1, 125.2, 126.3, 126.5, 129.5, 129.6, 129.8, 130.7 (C_{21}, C_{26}, C_{31}, C_{33}, C_{34}, C_{35}, C_{36}, C_{38}). FD-MS: *m*/*e* 540 (100, M^+). Anal. Calcd for $C_{42}H_{36}$: C, 93.28; H, 6.27. Found: C, 93.64; H, 6.68.

6.4. Synthesis of 3-(1-Pyrene)-8,11-di(*tert*-butyl)perylene (5). Similar to the synthesis of **3** and **4**, the formation of the boronic acid was performed. An amount of 1.4 mL of *n*-butyllithium (1.6 M/hexane) was added to 570 mg (2.03 mmol) of 1-bromopyrene in THF at −78 °C. After being stirred for 15 min, the mixture was allowed to warm to 0 °C. Then 0.19 mL of boronic acid trimethyl ester was added to form the 1-pyrenylboronic acid. After 20 min, the mixture was quenched with 0.01 M HCl. The solvents were removed under reduced pressure, and the crude product was recrystallized from water. An amount of 200 mg (0.81 mmol) of the resulting product dissolved in 40 mL of ethanol, and this was added to a mixture of 10 mmol of sodium carbonate in 20 mL of water and 360 mg (0.81 mmol) of 3-bromo-8,11-di(*tert*-butyl)perylene in 40 mL of toluene. The last compound was prepared by methods described in the literature.[17] After the addition of 40 mg of tetrakis(triphenylphosphine)palladium(0), degassing of the solvent with argon, and the exclusion of light, the reaction mixture was heated to 115 °C for 30 h. The solvent was removed under reduced pressure, and the resulting residue was purified by chromatography (silica gel/*n*-pentane). 0.390 g of the product **5** was obtained (i.e., 82% yield).

^{1}H NMR (500 MHz, $CDCl_3$), δ: 1.45 (s, 9H), 1.43 (s, 9H); ($3H_{22}$, $3H_{23}$, $3H_{24}$ o. $3H_{26}$, $3H_{27}$, $3H_{28}$); 8.35 (d, ^3J(H, H) = 7.6 Hz, 1H), 7.54 (d, ^3J(H, H) = 7.6 Hz, 1H); (H_2, H_1); 8.32 (s, 1H), 8.24 (s, 1H); (H_9, H_{10}); 8.22 (d, ^3J(H, H) = 7.2 Hz, 1H), 7.99 (d, ^3J(H, H) = 7.5 Hz, 1H); (H_{30}, H_{31} o. H_{32}, H_{33} o. H_{37}, H_{38}); 8.17 (d, ^3J(H, H) = 7.0 Hz, 1H), 7.18 (m (d), 1H); (H_6, H_4); 8.14 (d, ^3J(h, H) = 7.6 Hz, 1H), 8.08 (m (d), 1H); (H_{34}, H_{36}); 8.08 (m (d), 1H), 8.08 (m (d), 1H); (H_{30}, H_{31} o. H_{32}, H_{33} o. H_{37}, H_{38}); 7.94 (dd, $^3J_1$(H, H) = 7.6 Hz, $^3J_2$(H, H) = 7.4 Hz, 1H); (H_{35}); 7.84 (d, ^3J(H, H) = 9.2 Hz, 1H), 7.71 (d, ^3J(H, H) = 9.1 Hz, 1H); (H_{31}, H_{31} o. H_{32}, H_{33} o. H_{37}, H_{38}); 7.63 (s, 2H); (H_7, H_{12}); 7.18 (m (dd), 1H); (H_2). ^{13}C NMR (500 MHz, $CDCl_3$), δ: 149.2 (C_3, C_{29}); 138.3, 136.1, 134.8, 134.5, 131.8, 131.5, 131.4, 131.1, 130.9, 130.6, 130.5, 129.9, 129.3, 125.4 (C_8, C_{11}, C_{13}, C_{14}, C_{15}, C_{16}, C_{18}, C_{19}, C_{20}, C_{39}, C_{40}, C_{42}, C_{44}); 125.2, 125.2 (C_{41}, C_{43}); 37.4, 37.4 (C_{21}, C_{25}); 129.1, 128.3, 127.4, 126.5, 126.4, 126.0, 125.8, 125.4, 125.2, 124.6, 123.6, 123.6, 120.0, 119.5, 118.6, 118.4 (C_1, C_2, C_4, C_5, C_6, C_7, C_{12}, C_{30}, C_{31}, C_{32}, C_{33}, C_{34}, C_{35}, C_{36}, C_{37}, C_{38}). FD-MS: *m*/*e* 564 (100, M^+). Anal. Calcd for $C_{44}H_{36}$: C, 93.57; H, 6.43. Found: C, 93.49; H, 6.89. mp: 255 °C.

Acknowledgment. M.B. and W.R. gratefully acknowledge support from Stiftung Volkswagenwerk, Project VW 69641. M.B. also thanks the Fond der chemischen Industrie.

References and Notes

(1) *Handbook of Conducting Polymers*; Skotheim, T. A., Ed.; Marcel Dekker: New York, 1986. *Handbook of Conducting Polymers*; Skotheim, T. A., Ed.; Marcel Dekker: New York, 1997.
(2) *Conjugated Polymers*; Brédas, J. L., Silbey, R., Eds.; Kluwer Academic Publishers: Dordrecht, 1991.
(3) Baumgarten, M.; Müllen, K. *Top. Curr. Chem.* **1994**, *169*, 1.
(4) Baumgarten, M.; Huber, W.; Müllen, K. *Adv. Phys. Org. Chem.* **1993**, *28*, 1.
(5) (a) Müller, U.; Baumgarten, M. *J. Am. Chem. Soc.* **1995**, *117*, 5840. (b) Baumgarten, M.; Müller, U.; Bohnen, A.; Müllen, K. *Angew. Chem.* **1992**, *104*, 482.
(6) Naarmann, H. *Angew. Makromol. Chem.* **1982**, *109*, 295.
(7) Müllen, K. *Pure Appl. Chem.* **1993**, *65*, 89.
(8) (a) Kreyenschmidt, M.; Baumgarten, M.; Tyutyulkov, N.; Müllen, K. *Angew. Chem.* **1994**, *106*, 2062 (*Angew. Chem., Int. Ed. Engl.* **1994**, *33*, 1957). (b) Kreyenschmidt, M. Ph.D. Thesis, Johannes Gutenberg−Universität Mainz, Mainz, Germany, 1995.
(9) Mazur, S.; Dixit, V. M.; Gerson, F. *J. Am. Chem. Soc.* **1980**, *102*, 5343.
(10) Movaghar, B. *J. Mol. Electron.* **1987**, *3*, 183.
(11) Andrieux, C. P.; Saveant, J. M. *J. Chem. Phys.* **1988**, *92*, 6761.
(12) Heitele, H. *Angew. Chem.* **1993**, *105*, 378.
(13) Marcus, R. A. *J. Chem. Phys* **1965**, *43*, 679.
(14) Gloss, G. L.; Miller, J. R. *Science* **1988**, *240*, 440.
(15) (a) Grampp, G.; Kapturkiewicz, A.; Saalbeck, J. *J. Chem. Phys.* **1994**, *187*, 391. (b) Friedrich, J. Ph.D. Thesis, Johannes Gutenberg−Universität Mainz, Mainz, Germany, 1997. (c) Friedrich, J.; Baumgarten, M. *Appl. Magn. Reson.* **1997**, *13*, 393.
(16) (a) Gerson, F.; Wellauer, T.; Oliver, A. M.; Paddon Row, M. N. *Helv. Chim. Acta* **1990**, *73*, 1586. (b) Gerson, F.; Huber, W.; Martin, W. B.; Caluwe, P.; Pepper, T.; Szwarc, M. *Helv. Chim. Acta* **1984**, *94*, 871.
(17) (a) Suzuki, M.; Saweda, S.; Saegusa, T. *Macromolecules* **1989**, *22*, 1505. (b) Rehahn, M.; Schlüter, A. D.; Wegner, G. *Macromol. Chem.* **1990**, *191*, 1991.
(18) Biehl, R.; Hinrichs, K.; Kurreck, H.; Lubitz, W.; Mennenga, U.; Roth, K. *J. Am. Chem. Soc.* **1977**, *99*, 4278.
(19) Baumgarten, M.; Koch, K. H.; Müllen, K. *J. Am. Chem. Soc.* **1994**, *116*, 7341.
(20) Carrington, A.; McLachlan, A. D. *Introduction to Magnetic Resonance*; Harper & Row: New York, 1967; p 130.
(21) Weil, J. A.; Bolton, J. R.; Wertz, J. E. *Electron Paramagnetic Resonance*; Wiley: New York, 1994.
(22) (a) Carrington, A.; Dravnieks, F.; Symons, M. C. R. *J. Chem. Soc.* **1959**, 947. (b) Colpa, J. P.; Bolton, J. R. *Mol. Phys.* **1963**, *6*, 273. (c) Bolton, J. R. *J. Chem. Phys.* **1965**, *43*, 309.
(23) Friedrich, J.; Baumgarten, M. *Appl. Magn. Reson.* **1997**, *13*, 393.
(24) Kapturkiewicz, A.; Herbich, J. *J. Am. Chem. Soc.* **1998**, *120*, 1014.
(25) Oevering, H.; Verhoeven, J. W.; Paddon-Row, M. N.; Warman, J. M. *Tetrahedron* **1989**, *45*, 4751.
(26) Rettig, W. *Angew. Chem., Int. Ed. Engl.* **1986**, *25*, 971.
(27) Rettig, W.; Zander, M. *Ber. Bunsen-Ges. Phys. Chem.* **1983**, *87*, 1143.
(28) Schneider, F.; Lippert, E. *Ber. Bunsen-Ges. Phys. Chem.* **1968**, *72*, 1155.
(29) Nakashima, N.; Murakawa, M.; Mataga, M. *Bull. Chem. Soc. Jpn.* **1976**, *49*, 854.
(30) Schütz, M.; Schmidt, R. *J. Phys. Chem.* **1996**, *110*, 2012.
(31) Grabowski, Z. R.; Dobkowski, J. *Pure Appl. Chem.* **1983**, *55*, 245.
(32) Catalan, J.; Diaz, C.; Lopez, V.; Perez, P.; Claramunt, R. M. *J. Phys. Chem.* **1996**, *100*, 18392.
(33) Dobkowski, J.; Grabowski, Z. R.; Paeplow, B.; Rettig, W.; Koch, K. H.; Müllen, K.; Lapouyade, R. *New J. Chem.* **1994**, *18*, 525.
(34) (a) Subaric-Leitis, A.; Monte, C.; Roggan, A.; Rettig, W.; Zim-

mermann, P.; Heinze, J. *J. Chem. Phys*. **1990**, *93*, 4543. (b) Zander, M.; Rettig, W.; *Chem. Phys. Lett*. **1984**, *110*, 602. (c) Birks, J. B. *Photophysics of Aromatic Molecules*; Wiley-Interscience: London, New York, 1970.

(35) Beens, H.; Weller, A. *Organic Molecular Photophysics*; Wiley-Interscience: London, 1975; Vol. 2, p 159.

(36) McConnell, H. M. *J. Chem. Phys.* **1956**, *24*, 632.

(37) Gerson, F. *High-resolution ESR spectroscopy*; VCH: Weinheim, 1970.

(38) Fritz, R.; Rettig, W.; Nishiyama, K.; Okada, T.; Müller, W.; Müllen, K.; *J. Phys. Chem. A* **1997**, *101*, 2796.

(39) Stolarczyk, L.; Piela, L. *Chem. Phys.* **1984**, *85*, 451.

(40) Velapoldi, R. A.; Epstein, M. S. *ACS Symp. Ser*. **1989**, *383*, 98.

(41) O'Connor, D. V.; Phillips, D. *Time Correlated Single Photon Counting*; Academic Press: London, 1984.

(42) Vogel, M.; Rettig, W. *Ber. Bunsen-Ges. Phys. Chem*. **1987**, *91*, 1241.